To be published in Journal of the Optical Society of America A:

Title:	Determining the Size and Refractive Index of Microspheres using the Mode Assignments from Mie Resonances
Authors:	Thomas Preston and Jonathan Reid
Accepted:	25 September 2015
Posted:	28 September 2015
Doc. ID:	245515

Determining the Size and Refractive Index of Microspheres using the Mode Assignments from Mie Resonances

September 8, 2015

Thomas C. Preston*[a] and Jonathan P. Reid[b]

[a]*Department of Atmospheric and Oceanic Sciences and Department of Chemistry, McGill University, 805 Sherbrooke Street West, Montreal, QC, Canada H3A 0B9*

[b]*School of Chemistry, University of Bristol, Cantock's Close, Bristol, UK, BS8 1TS*

submitted to the Journal of the Optical Society of America A

5 Figures, 1 Appendix and 17 manuscript pages

* Thomas C. Preston

e-mail: thomas.preston@mcgill.ca

Abstract

A new method for determining the radius and refractive index of microspheres using Mie resonances is presented. Previous methods have relied on searching a multidimensional space in order to find the radius and refractive index that minimize the difference between observed and calculated Mie resonances. For anything but simple refractive index functions this process can be very time consuming. Here, we demonstrate that once the mode assignment for the observed Mie resonances is known, no search is necessary and the radius and refractive index of best-fit can be found immediately. This superior and faster way to characterize microspheres using Mie resonances should supplant previous fitting algorithms. The derivation and implementation of the equations that give the parameters of best-fit are shown and discussed. Testing is performed on systems of physical interest and the effect of noise on measured peak positions is investigated.

OCIS Codes: (140.4780) Optical resonators; (260.2030) Dispersion; (290.3030) Index measurements; (290.4020) Mie theory

1 Introduction

Dielectric spheres can support electromagnetic modes and, when attenuation is weak, act as high-quality factor optical cavities.[1] For modes within the limit of total internal reflection, the resonance linewidth can be extremely narrow with a position that is very sensitive to both the size and the relative refractive index of a sphere. For plane wave scattering by a sphere, Mie theory[2] can be used to calculate resonance position, linewidth, and strength,[3,4] and each mode can be associated with an individual term in the Mie series. Resonances are commonly referred to as Mie resonances, morphology-dependent resonances (MDRs) or whispering gallery mode (WGM) resonances.

In an ensemble of spherical particles, even a small distribution in either size or refractive index will result in an averaging out of the characteristic features of sharp resonances in the scattering. Consequently, in typical measurements of aerosol or colloidal particles, one would not expect to observe such sharp peaks in extinction spectra. The most practical situation where such resonances can be observed is in the study of single particles. Indeed, it was not until optical trapping allowed for the spectra of single micrometer-sized particles to be measured that sharp peaks could be readily observed. An early example of such an observation was in single particle radiation pressure measurements performed at optical frequencies (where the observed ripple structure was associated with resonances in the Mie scattering coefficients).[5,6] There have since been many observations of sharp Mie resonances in optical trapping experiments, experiments using droplet generators, microcavities fabricated for photonic applications, and a variety of other systems.[4,7–17]

The sensitivity of resonances to changes in either the size or relative refractive index means

that spherical particles can be characterized with an extremely high precision (e.g. in a typical experiment, a sphere with a radius of several micrometers can be determined with an uncertainty of ± 0.001 μm).[18] Utilizing these resonances to simultaneously determine both the size and the relative refractive index of a sphere is an extremely powerful method to study single particles. For instance, in atmospheric science, the ability to characterize single particles using sharp electromagnetic resonances enables detailed studies of the thermodynamics and kinetics of surrogates of atmospheric aerosol as it allows changes to particle size and composition to be tracked in real-time with great accuracy.[19–23]

Several procedures for fitting observed Mie resonances in order to characterize particles have been presented in the literature.[4,18,20,24,25] Despite minor differences in approach, at their core these algorithms all rely on the same method to find the parameters of best-fit: (i) generate a library of simulated modes across a range of physically plausible parameters and then (ii) search for the parameters that minimize the difference between the observed and calculated modes (i.e. seek the parameters of best-fit). The function that is minimized in step (ii) is typically the sum of the squares of the differences between the observed and calculated modes. In these algorithms, it is common to assume that the refractive index is known beforehand or takes on a simple form, such as being a constant or a linear function of wavenumber ($\nu = 1/\lambda$).[4,18] Computational time necessitates this assumption as each unknown that is included in a refractive index function will add a further dimension to the search space (the function being minimized describes a hypersurface in a multidimensional space). Therefore, while fitting elaborate refractive index functions may be desirable, it is often not practical.

The previously referenced fitting algorithms are all designed around the idea of varying the parameters that describe the sphere (radius and refractive index) until the difference between

the observed and calculated modes is at a minimum. The parameters that give this minimum should, if the search is performed properly, be very close to the true radius and refractive index of the sphere. While prior knowledge of the correct mode assignment (mode number, order, and polarization) improves the overall speed of this fitting process, it does not fundamentally change it. Beyond constraining the search space, knowledge of the correct mode assignment is not used in this type of fitting.

In this report, we demonstrate that once a correct mode assignment is known for a sphere, no fitting is necessary and the parameters of best-fit can be found exactly. Just as the parameters of best-fit uniquely determine the mode assignment, the mode assignment can be used to uniquely determine the parameters of best-fit when the error between the observed and calculated modes is minimized. This represents a fundamentally new method for finding the parameters of best-fit and one that has a major advantage over previous algorithms. The most important difference is that for a system where the error needs to be minimized with respect to N parameters, it is not necessary to search an N-dimensional space to find the best-fit. This is because the parameters are found by solving a system of linear equations where the number of unknowns will be equal to the number of parameters to be fit. So, for example, if both the radius and refractive index of the sphere are unknown and the refractive index function is described by the Cauchy equation[26] (i.e. $m = m_0 + m_1/\lambda^2 + m_2/\lambda^4$) then there are only four unknowns in the system of equations (the radius, m_0, m_1 and m_2). In this example, the small set of equations can be solved rapidly and the computation time will be negligible. This will always be true for refractive index parameterizations that are of physical interest. In contrast, a search across more than three parameters using the previously referenced algorithms would be very time consuming.

This paper is organized as follows: in Section 2, it is shown, using the method of least-squares, that the parameters of best-fit for a sphere can be found using the observed positions of Mie resonances and their mode assignment. Following this, in Section 3 we discuss the practical aspects of performing such calculations. In Section 4, a Fortran program based on the methods and equations outlined in Sections 2 and 3 is used to fit many different simulated mode sets from spheres with a wide range of refractive indices and radii. Additionally, the effect of noise on peak positions and its relationship to the calculated parameters of best-fit is investigated.

2 Determination of the Parameters of Best-Fit using the Method of Least Squares

2.1 General Case

For a set of J measured Mie resonance positions at wavenumbers ν_j^e that are to be fit with a set of calculated peaks $\nu_j(m,a)$ (that are functions of the relative refractive index m and radius a of the particle), the sum of squared residuals[27] can be written as

$$S = \sum_{j=1}^{J} \left(\nu_j^e - \nu_j(m,a)\right)^2 = \sum_j \left(\nu_j^e - \frac{x_j(m)}{2\pi a}\right)^2, \tag{1}$$

where the size parameter is $x_j(m) = 2\pi a \nu_j(m,a)$. To write Eq. 1 in a form that can be minimized with respect to m and a it is first necessary to use the approximation that, across a small region of m, the position x_j of each mode can be described as being linear with respect to m

$$x_j(m) = mq_j + b_j. \tag{2}$$

The refractive index m can be expanded as a power series in ν around the center of the spectrum ν_0

$$m = \sum_{k=0}^{K} m_k(\nu - \nu_0)^k. \tag{3}$$

Inserting Eq. 2 and Eq. 3 into Eq. 1 yields

$$S = \sum_j \left(\nu_j^e - \frac{(m_0 + m_1(\nu_j^e - \nu_0) + \cdots + m_K(\nu_j^e - \nu_0)^K)q_j + b_j}{2\pi a}\right)^2. \tag{4}$$

For compactness, throughout the remainder of this section each series $m_0 + m_1(\nu_j^e - \nu_0) + \cdots + m_K(\nu_j^e - \nu_0)^K$ will simply be written as m_j.

The values of a, m_0, m_1, ... , m_K that minimize Eq. 4 are found by first setting the partial derivatives $\partial S/\partial a$, $\partial S/\partial m_0$, $\partial S/\partial m_1$, ... , $\partial S/\partial m_K$ to zero,

$$\begin{aligned}
\frac{\partial S}{\partial a} &= 2\sum_j \left(\nu_j^e - \frac{m_j q_j + b_j}{2\pi a}\right)\left(\frac{m_j q_j + b_j}{2\pi a^2}\right) = 0,\\
\frac{\partial S}{\partial m_0} &= 2\sum_j \left(\nu_j^e - \frac{m_j q_j + b_j}{2\pi a}\right)\left(-\frac{q_j}{2\pi a}\right) = 0,\\
\frac{\partial S}{\partial m_1} &= 2\sum_j \left(\nu_j^e - \frac{m_j q_j + b_j}{2\pi a}\right)\left(-\frac{(\nu_j^e - \nu_0) q_j}{2\pi a}\right) = 0,\\
&\vdots\\
\frac{\partial S}{\partial m_K} &= 2\sum_j \left(\nu_j^e - \frac{m_j q_j + b_j}{2\pi a}\right)\left(-\frac{(\nu_j^e - \nu_0)^K q_j}{2\pi a}\right) = 0,
\end{aligned} \tag{5}$$

and rearranging them to form the following system of equations:

$$\begin{aligned}
&\sum_j \left(2\pi a\nu_j^e - (m_j q_j + b_j)\right)(m_j q_j + b_j) = 0,\\
&\sum_j \left(2\pi a\nu_j^e - (m_j q_j + b_j)\right) q_j = 0,\\
&\sum_j \left(2\pi a\nu_j^e - (m_j q_j + b_j)\right)(\nu_j^e - \nu_0) q_j = 0,\\
&\vdots\\
&\sum_j \left(2\pi a\nu_j^e - (m_j q_j + b_j)\right)(\nu_j^e - \nu_0)^K q_j = 0.
\end{aligned} \tag{6}$$

Solving this system of equations for a, m_0, m_1, ... , m_K has the algebraic difficulty that the expression derived from $\partial S/\partial a$ (the left-hand side of the first equation in system 6) contains terms such as m_0^2, $m_0 m_1$, ... , $m_0 m_K$, m_1^2, $m_1 m_2$, ... , $m_1 m_K$, etc. However, these can be removed by writing the expression as

$$\begin{aligned}
&m_0 \sum_j \left(2\pi a\nu_j^e - (m_j q_j + b_j)\right) q_j + m_1 \sum_j \left(2\pi a\nu_j^e - (m_j q_j + b_j)\right)(\nu_j^e - \nu_0) q_j\\
&+ \cdots + m_K \sum_j \left(2\pi a\nu_j^e - (m_j q_j + b_j)\right)(\nu_j^e - \nu_0)^K q_j + \sum_j \left(2\pi a\nu_j^e - (m_j q_j + b_j)\right) b_j
\end{aligned}$$

and recognizing that all of the summations except for the last one will be equal to zero during the minimization (i.e. the equations for $\partial S/\partial m_0$, $\partial S/\partial m_1$, ... , $\partial S/\partial m_K$ from system 6). The first equation in system 6 then simplifies to

$$\sum_j \left(2\pi a \nu_j^e - (m_j q_j + b_j)\right) b_j = 0$$

and system 6 is now a set of linear simultaneous equations. Defining the vectors

$$\mathbf{v} = (a, m_0, m_1, \ldots, m_K),$$

$$\mathbf{d} = \left(\sum_j b_j^2, \sum_j q_j b_j, \sum_j q_j b_j (\nu_j^e - \nu_0), \ldots, \sum_j q_j b_j (\nu_j^e - \nu_0)^K\right),$$

along with the matrix

$$\mathbf{A} = \begin{bmatrix} 2\pi \sum_j \nu_j^e b_j & -\sum_j q_j b_j & -\sum_j q_j b_j (\nu_j^e - \nu_0) & \cdots & -\sum_j q_j b_j (\nu_j^e - \nu_0)^K \\ 2\pi \sum_j \nu_j^e q_j & -\sum_j q_j^2 & -\sum_j q_j^2 (\nu_j^e - \nu_0) & \cdots & -\sum_j q_j^2 (\nu_j^e - \nu_0)^K \\ 2\pi \sum_j \nu_j^e q_j (\nu_j^e - \nu_0) & -\sum_j q_j^2 (\nu_j^e - \nu_0) & -\sum_j q_j^2 (\nu_j^e - \nu_0)^2 & \cdots & -\sum_j q_j^2 (\nu_j^e - \nu_0)^{K+1} \\ \vdots & \vdots & \vdots & \ddots & \vdots \\ 2\pi \sum_j \nu_j^e q_j (\nu_j^e - \nu_0)^K & -\sum_j q_j^2 (\nu_j^e - \nu_0)^K & -\sum_j q_j^2 (\nu_j^e - \nu_0)^{K+1} & \cdots & -\sum_j q_j^2 (\nu_j^e - \nu_0)^{2K} \end{bmatrix},$$

the equations can be compactly written as

$$\mathbf{A} \cdot \mathbf{v} = \mathbf{d}. \tag{7}$$

Therefore, the parameters of best-fit $\mathbf{v}$ can be found by solving the system of linear equations in Eq. 7.

Often Eq. 3 is not the preferred function for the refractive index and instead the form of the Cauchy equation,[26]

$$m = m_0 + m_1 \nu^2 + m_2 \nu^4 + \cdots + m_K \nu^{2K} = \sum_{k=0}^{K} m_k \nu^{2k}, \tag{8}$$

provides a more suitable description of dispersion. When Eq. 8 is used to expand the refractive index in Eq. 2 and the error minimization is subsequently performed, the vectors and matrix

in Eq. 7 will be

$$\mathbf{v} = (a, m_0, m_1, \ldots, m_K),$$

$$\mathbf{d} = \left(\sum_j b_j^2, \sum_j q_j b_j, \sum_j q_j b_j (\nu_j^e)^2, \ldots, \sum_j q_j b_j (\nu_j^e)^{2K} \right),$$

$$\mathbf{A} = \begin{bmatrix} 2\pi \sum_j \nu_j^e b_j & -\sum_j q_j b_j & -\sum_j q_j b_j (\nu_j^e)^2 & \cdots & -\sum_j q_j b_j (\nu_j^e)^{2K} \\ 2\pi \sum_j \nu_j^e q_j & -\sum_j q_j^2 & -\sum_j q_j^2 (\nu_j^e)^2 & \cdots & -\sum_j q_j^2 (\nu_j^e)^{2K} \\ 2\pi \sum_j \nu_j^e q_j (\nu_j^e)^2 & -\sum_j q_j^2 (\nu_j^e)^2 & -\sum_j q_j^2 (\nu_j^e)^4 & \cdots & -\sum_j q_j^2 (\nu_j^e)^{2K+2} \\ \vdots & \vdots & \vdots & \ddots & \vdots \\ 2\pi \sum_j \nu_j^e q_j (\nu_j^e)^{2K} & -\sum_j q_j^2 (\nu_j^e)^{2K} & -\sum_j q_j^2 (\nu_j^e)^{2K+2} & \cdots & -\sum_j q_j^2 (\nu_j^e)^{4K} \end{bmatrix}.$$

2.2 Special Cases

In Section 2.1, the best-fits were found when no parameters were known beforehand. For the special case when a is already known, the minimization process shown above can be greatly simplified. In this situation, ψ can be defined as

$$\psi = 2\pi a S = \sum_{j=1}^{J} \left(c_j - \sum_{k=0}^{K} r_{jk} m_k \right)^2, \tag{9}$$

where $c_j = 2\pi a \nu_j^e - b_j$ and $r_{jk} = (\nu_j^e - \nu_0)^k q_j$. The function ψ is minimized when

$$\frac{\partial \psi}{\partial m_l} = 2 \sum_{j=1}^{J} \left(c_j - \sum_{k=0}^{K} r_{jk} m_k \right) (-r_{jl}) = 0, \quad \text{where } l = 0, 1, \ldots, K. \tag{10}$$

This system of equations can be rearranged to obtain the normal equations for the linear least squares problem:

$$\sum_{j=1}^{J} r_{jl} \sum_{k=0}^{K} r_{jk} m_k = \sum_{j=1}^{J} r_{jl} c_j, \quad \text{where } l = 0, 1, \ldots, K. \tag{11}$$

In matrix form the normal equations will be

$$(\mathbf{R^T R})\mathbf{m} = \mathbf{R^T c}. \tag{12}$$

The advantage that Eq. 12 has over Eq. 7 is that $\mathbf{R^T R}$ will be positive-definite whereas, in general, $\mathbf{A}$ will not be positive-definite. Therefore, Cholesky decomposition can be used when solving Eq. 12 but not Eq. 7. Of course, in most situations of practical interest a will not be known with sufficient accuracy to apply Eq. 12 and retrieve accurate values of m.

There is one other special case to consider and that is when m is a known function of ν. Here, the a of best-fit can be found by solving the first equation in system 6:

$$a = \frac{\sum_j (m_j q_j + b_j)^2}{2\pi \sum_j \nu_j^e (m_j q_j + b_j)} \tag{13}$$

This equation is potentially useful in cases where the m is well characterized and the number of observable modes is low.

For the remainder of this work we will focus on the implementation of Eq. 7. However, all the methods that will be described here can be applied to Eq. 12 and 13.

3 Calculating the Parameters of Best-fit

To calculate $\mathbf{v}$ from Eq. 7 the values of q_j and b_j for each ν_j^e are required. For a mode j, the values of q_j and b_j across a range of m can be found numerically by first calculating the resonant size parameter x_j over a refractive index grid in steps of Δ and then using the equations

$$q_j(m) = \frac{x_j(m+\Delta) - x_j(m-\Delta)}{2\Delta}, \tag{14}$$

$$b_j(m) = x_j(m) - mq_j(m). \tag{15}$$

Very accurate results can be achieved using $\Delta = 0.005$ as x_j is approximately a linear function of m over fairly large ranges of m. As an example, Fig. 1 shows several resonant size parameters from $m = 1.4$ to 1.5. Linear interpolation can then be used to quickly find q_j or b_j at any value of m within the bounds of the grid.

To use Eqs. 14 and 15, values of x_j must first be calculated. An accurate method to accomplish this has been discussed previously[4,18] and is reviewed here. Resonances occur at the poles of the Mie scattering coefficients, thus the characteristic equation can be found by setting the denominators of the coefficients to zero. The resonance condition for both transverse electric (TE) and transverse magnetic (TM) polarizations can be written as[28–31]

$$mp\frac{j_n'(mz)}{j_n(mz)} = \frac{h_n^{(1)\prime}(z)}{h_n^{(1)}(z)} + \frac{1-p}{z}, \tag{16}$$

where the functions $h_n^{(1)} = j_n + iy_n$, j_n, and y_n are spherical Bessel functions, $p = 1$ for TE polarization, $p = 1/m^2$ for TM polarization, and z is the complex size parameter. Solutions to Eq. 16 yield complex resonant size parameters $z_j = x_j + iy_j$, where the real part x_j will be the resonance position and the imaginary part y_j can be used to calculate the full width at half

maximum of the resonance Γ_j through the relationship $y_j = -\Gamma_j/2$.[3] Note: do not confuse y_j with the spherical Bessel function y_n.

When using a root-finding algorithm like the Newton-Raphson method to find solutions to Eq. 16, it is necessary to already have a satisfactory guess for z_j. This is because, even when n and t are fixed, the function

$$f(z) = mp\frac{j_n'(mz)}{j_n(mz)} - \frac{h_n^{(1)\prime}(z)}{h_n^{(1)}(z)} - \frac{1-p}{z} \tag{17}$$

still has an infinite number of roots and identifying which root corresponds to the l of interest is not trivial. One method to obtain a suitable initial guess is to use the explicit asymptotic formula for the resonance positions derived by Lam *et al.*:[3]

$$mx_j = \eta + \alpha_l \left(\frac{\eta}{2}\right)^{1/3} + \sum_{k=0}^{\infty} \frac{c_k(\alpha_l, m, t)}{\eta^{k/3}}, \tag{18}$$

where $\eta = n + 1/2$, α_l are the roots of the Airy function $\mathrm{Ai}(-x)$, and the coefficients $c_k(\alpha_l, m, t)$ are solved using the method described in Ref. 3. The coefficients c_0 through c_6 are listed in Appendix A. Using any coefficients beyond these provides little to no improvement in the accuracy of the resonance positions calculated using Eq. 18 and is unnecessary when treating the calculated positions as initial guesses for Eq. 16. Finally, Eq. 18 should only be used if the condition for total internal reflection, $x < n + \frac{1}{2}$, is satisfied.

Using the values of q_j and b_j calculated from Eqs. 14 and 15 with the equations given in Section 2 requires that the correct mode assignment is known (the mode number n, order l, and polarization t for each ν_j^e). In principle, the correct assignment can be found by calculating S for every possible mode combination within a range of n and l. The mode combination that gives the lowest value of S will then be the correct assignment. However, in most situations this approach is not practical. Consider a case where there are 12 experimentally measured modes

whose assignments are unknown. If the search space when assigning these modes includes values of n ranging from 30 to 70, values of l ranging from 1 to 2, and both TE and TM polarizations (the values of t) the number of possible mode combinations that needs to be considered is approximately 5.23×10^{17}. Calculating S for each mode combination across this fairly typical search space is not feasible. Even if assumptions are made to reduce the search space, it will be difficult to reduce its size to a point where such a search becomes practical.

An alternative method is therefore needed to assign modes. In this work, mode assignments are determined by assuming that the refractive index is a linear function of ν and fitting the modes using a previously described algorithm.[18] In Section 4, it is shown that this method produces the correct mode assignment for a physically relevant refractive index that is not well-described as being a linear function of ν.

4 Testing

An algorithm based around the equations and methods from Sections 2 and 3 was implemented using Fortran. The accuracy of the parameters of best-fit calculated using Eq. 7 was tested using simulated mode sets that were generated by randomly assigning the parameters a, m_0, m_1, m_2, and m_3 while using the refractive index function from Eq. 3. Values of a were restricted from 3 to 6 μm and the values m_0, m_1, m_2, and m_3 were such that the function m was always between 1.30 and 1.60 for $\lambda = 0.4$ to 0.7 μm. For simplicity and to match situations of physical interest, only m that increased monotonically with ν were used. 10,000 simulated mode sets were generated. For each set, only modes with $l = 1$ and 2 were included. After fitting all of these sets, the relative error in radius, $\delta a = (a_{\text{best-fit}} - a_{\text{true}})/a_{\text{true}}$, and refractive index, $\delta m = (m_{\text{best-fit}} - m_{\text{true}})/m_{\text{true}}$, were calculated for each set (the value of m at $\lambda = 0.55$ μm was used when calculating δm) and are shown in Fig. 2. For the 10,000 mode sets, the standard deviation in δa was 4.3×10^{-8} and the standard deviation in δm was 4.4×10^{-8}. These results correspond to an uncertainty in a of $\pm 1.9 \times 10^{-7}$ μm when $a = 4.5$ μm and an uncertainty in m of $\pm 6.3 \times 10^{-8}$ when $m = 1.45$. As these uncertainties are extremely low, this means that the uncertainty associated with measuring peak positions will determine the precision of the retrieved radii and refractive indices from real systems (discussed below).

As a second test, the fitting of simulated Mie scattering spectra from polystyrene spheres were considered. Fig. 3 shows the extinction efficiency, Q_{ext}, calculated across a wavelength range found in typical optical trapping experiments,[17] for spheres where $a = 3$ and 6 μm. For both spheres, the refractive index function was chosen to be[25]

$$m = m_0 + \frac{m_1}{\lambda^2} + \frac{m_2}{\lambda^4},$$

where $m_0 = 1.5656$, $m_1 = 0.00785$ μm^2, and $m_2 = 0.000334$ μm^4.

When fitting the peak positions with the algorithm, only peaks with full width at half maxima that were less than 10^{-4} μm were used and peak positions were refined prior to analysis using parabolic interpolation. The mode assignment was not assumed to be known and was instead found using the method described in Section 3. For both spheres, the mode assignments were correctly identified. Fig. 4a and b compare the true m to the m of best-fit for both of the spheres. Fig. 4a shows the m of best-fit over the wavelength range that contained the fitted modes. In this range, the agreement between the fitted and the true m is excellent. Interestingly, Fig. 4b shows that good agreement is also seen outside of the range that contained the fitted modes. For the $a = 3$ and 6 μm spheres, the a of best-fit were 2.99989 and 5.99997 μm, respectively. Therefore, in both cases, the refractive index and radius of best-fit are in excellent agreement with the true refractive index and radius.

The effect of adding noise to the calculated peaks prior to fitting was explored. Fig. 5 shows the relative uncertainty in a and m as Gaussian noise with a standard deviation of σ_g was added to the peak positions retrieved from simulated Q_{ext} plots for spheres where $a = 3$ and 6 μm. Sample distributions used to calculate the relative uncertainties were found by applying Gaussian noise with σ_g to 1000 identical modes sets and subsequently generating 1000 noisy mode sets. These noisy sets were then fitted and the resulting parameters of best-fit were used to calculate the standard deviations and means necessary to find the relative uncertainties. In both Fig. 5a and b, the relative uncertainties are linear with σ_g and have very similar values across the chosen range of σ_g. An example of a previously reported uncertainty associated with fitting WGM wavlengths on a spectrograph is $\pm 10^{-5}$ μm.[20] For $a = 3.0$ μm, this gives an uncertainty in a of ± 0.0011 μm and an uncertainty in m of ± 0.00063 and, for $a = 6.0$ μm, an

uncertainty in a of ± 0.0019 μm and an uncertainty in m of ± 0.00052. These uncertainties are similar to what we have reported earlier.[18]

Additional testing of the algorithm was performed on several other data sets. First, the peak positions listed in Tables 1 and 2 from Ref. 4 were fitted using the refractive index function $m = m_0 + m_1(\nu - \nu_0)$, where $\nu_0 = 17000$ cm^{-1} (the same function used in Ref. 4). For data set A from that work, our best-fit was $a = 7.139$ μm, $m_0 = 1.366$, and $m_1 = 1.012 \times 10^{-6}$ cm^{-1}. For data set B from that work, our best-fit was $a = 7.658$ μm, $m_0 = 1.364$, and $m_1 = 1.081 \times 10^{-6}$ cm^{-1}. Both of these results are in good agreement with the best-fits from Ref. 4 (data set A: $a = 7.133$ μm, $m_0 = 1.366$, and $m_1 = 0.964 \times 10^{-6}$ cm^{-1} and data set B: $a = 7.652$ μm, $m_0 = 1.365$, and $m_1 = 1.06 \times 10^{-6}$ cm^{-1}). Secondly, many simulated mode sets that contained large n and l (n up to 400 and l up to 25) were fitted. No new difficulties were encountered fitting such sets. Finally, as the fitting of resonances from microspheres in media that have a refractive index that is greater than one are of significant interest,[32–34] simulated mode sets from such systems were fitted here. It was found that in order to obtain accurate parameters of best-fit using the solution from Section 2.1, the refractive index of the medium needs to be well-known.

5 Conclusion

We have presented a solution to the problem of determining the size and refractive index of microspheres using Mie resonances. Once the mode assignment is known, the parameters of best-fit can quickly be found by solving a system of linear equations. The application of this method was discussed in detail and tested using simulated mode sets for spheres over a range of physically relevant sizes and refractive indices. A Fortran implementation of the Mie resonance

fitting method, a program called MRFIT, has been developed by the authors and will be made freely available.

Acknowledgements

T.C.P. acknowledges support from the Natural Sciences and Engineering Research Council of Canada (NSERC). J.P.R. acknowledges the Engineering and Physical Sciences Research Council (EPSRC) for support as a Leadership Fellow.

Appendix A

For Eq. 18 the coefficients c_0 through c_6 are:

$$c_0 = -\frac{mp}{(m^2-1)^{1/2}},$$

$$c_1 = \frac{3\alpha_l^2}{10(2^{2/3})},$$

$$c_2 = \frac{\alpha_l m^3 p(2p^2-3)}{3(2^{1/3})(m^2-1)^{3/2}},$$

$$c_3 = \frac{10-\alpha_l^3-20m^2+2\alpha_l^3m^2+10m^4-\alpha_l^3m^4-350m^4p+700m^4p^2-350m^4p^4}{700(m^2-1)^2},$$

$$c_4 = -\frac{\alpha_l^2 m^3 p(12+3m^2-8p^2-12m^2p^2+8m^2p^4)}{10(2^{2/3})(m^2-1)^{5/2}},$$

$$\begin{aligned} c_5 = &-[\alpha_l(-40-479\alpha_l^3+120m^2+1437\alpha_l^3m^2-120m^4-1437\alpha_l^3m^4+40m^6+479\alpha_l^3m^6 \\ &+189000m^4p+63000m^6p-378000m^4p^2-126000m^6p^2-126000m^6p^3 \\ &+189000m^4p^4+399000m^6p^4-196000m^6p^6)]/[126000(2^{1/3})(m^2-1)^3], \end{aligned}$$

$$\begin{aligned} c_6 = &[m^3p(-195-768\alpha_l^3-660m^2-984\alpha_l^3m^2-370m^4+2\alpha_l^3m^4+2100m^2p+1400m^4p+130p^2 \\ &+512\alpha_l^3p^2-2360m^2p^2+2336\alpha_l^3m^2p^2-1270m^4p^2+652\alpha_l^3m^4p^2-1400m^4p^3+840m^2p^4 \\ &-1344\alpha_l^3m^2p^4+2660m^4p^4-1456\alpha_l^3m^4p^4-1000m^4p^6+800\alpha_l^3m^4p^6)]/[1400(m^2-1)^{7/2}]. \end{aligned}$$

The definitions of p, m, and α_l are given in Section 3.

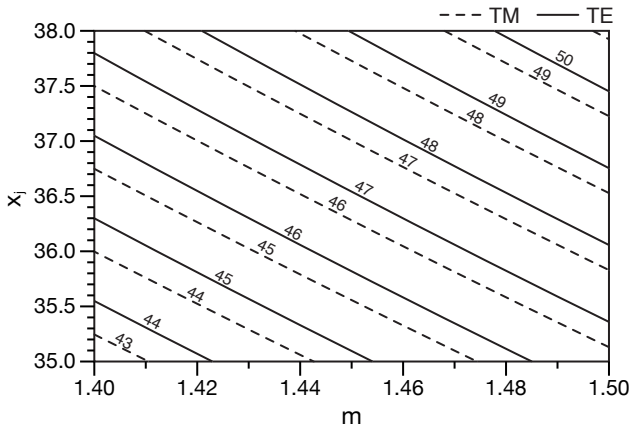

Figure 1: Example of x_j as a function of m for first order modes.

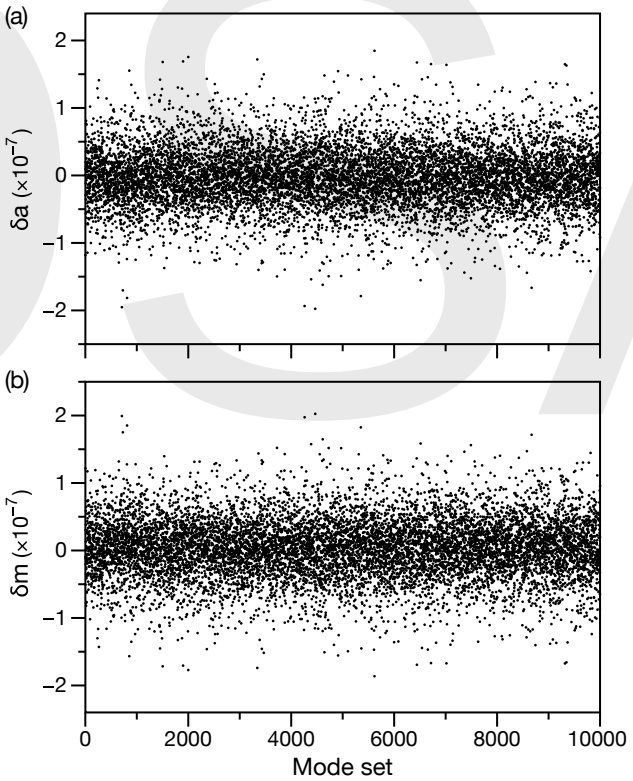

Figure 2: Relative errors for (a) a and (b) m (at $\lambda = 0.55$ μm) calculated using the best-fits from 10,000 simulated mode sets (see Section 4 for details). The relative errors are defined as $\delta a = (a_{\text{best-fit}} - a_{\text{true}})/a_{\text{true}}$ and $\delta m = (m_{\text{best-fit}} - m_{\text{true}})/m_{\text{true}}$.

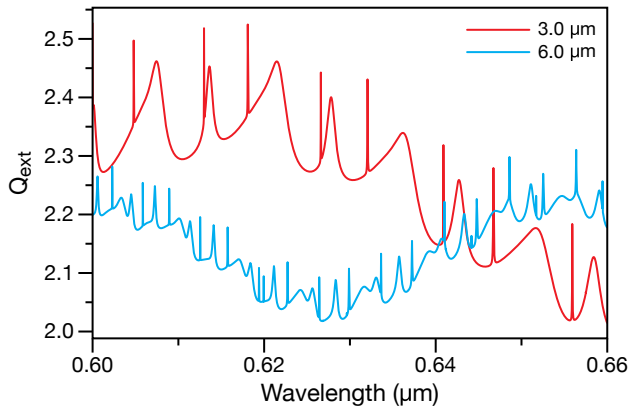

Figure 3: Extinction efficiency curves for polystyrene spheres calculated using Mie theory. When calculating each curve, a step size of 10^{-5} μm was used across the wavelength range of 0.60 to 0.66 μm.

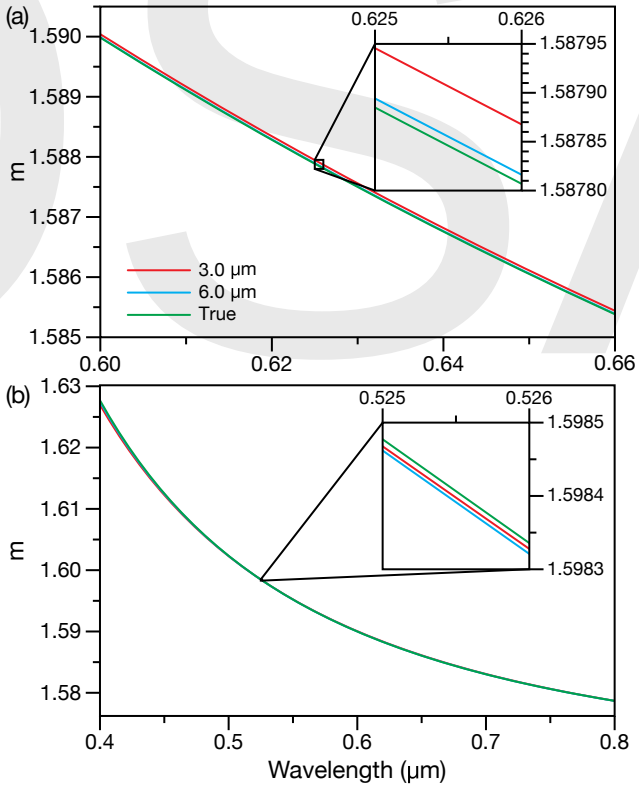

Figure 4: Comparison between the true and fitted m for polystyrene spheres (whose spectra are shown in Fig. 3).

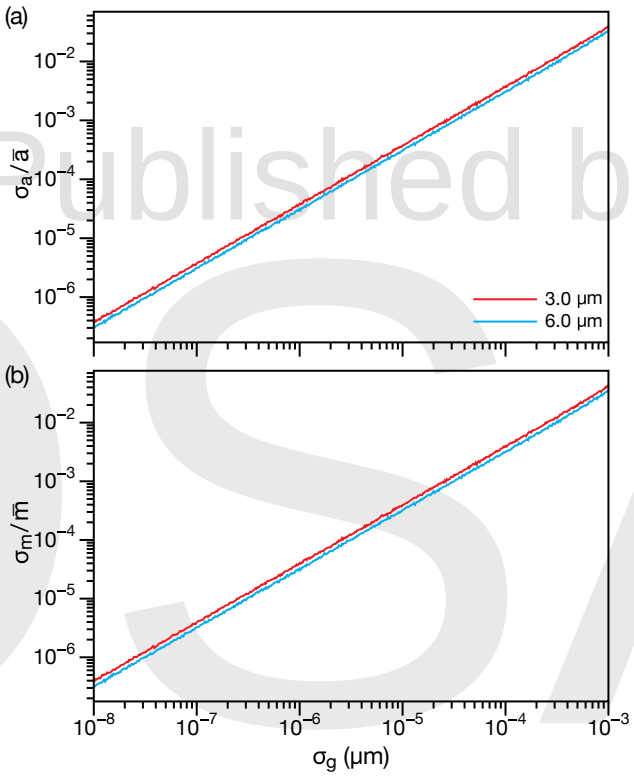

Figure 5: The relative uncertainty for (a) a and (b) m (at $\lambda = 0.63$ μm) as a function of σ_g when fitting the peak positions of polystyrene spheres (whose spectra are shown in Fig. 3). See Section 4 for the details of these calculations.

References

1. R. D. Richtmyer, "Dielectric resonators," J. Appl. Phys. **10**, 391-398 (1939).

2. G. Mie, "Beiträge zur optik trüber medien, speziell kolloidaler metallösungen," Ann. Phys. **330**, 377-445 (1908).

3. C. Lam, P. Leung, and K. Young, "Explicit asymptotic formulas for the positions, widths, and strengths of resonances in Mie scattering," J. Opt. Soc. Am. B **9**, 1585-1592 (1992).

4. J. D. Eversole, H. B. Lin, A. L. Huston, A. J. Campillo, P. T. Leung, S. Y. Liu, and K. Young, "High-precision identification of morphology-dependent resonances in optical processes in microdroplets," J. Opt. Soc. Am. B **10**, 1955-1968 (1993).

5. A. Ashkin and J. M. Dziedzic, "Observation of resonances in the radiation pressure on dielectric spheres," Phys. Rev. Lett. **38**, 1351-1354 (1977).

6. P. Chýlek, J. T. Kiehl, and M. K. W. Ko, "Optical levitation and partial-wave resonances," Phys. Rev. A **18**, 2229-2233 (1978).

7. R. E. Benner, P. W. Barber, J. F. Owen, and R. K. Chang, "Observation of structure resonances in the fluorescence spectra from microspheres," Phys. Rev. Lett. **44**, 475-478 (1980).

8. A. Ashkin and J. M. Dziedzic, "Observation of optical resonances of dielectric spheres by light scattering," Appl. Opt. **20**, 1803-1814 (1981).

9. J. F. Owen, R. K. Chang, and P. W. Barber, "Morphologydependent resonances in Raman scattering, fluorescence emission, and elastic scattering from microparticles," Aerosol Sci. Technol. **1**, 293-302 (1982).

10. S. C. Hill, R. E. Benner, C. K. Rushforth, and P. R. Conwell, "Structural resonances observed in the fluorescence emission from small spheres on substrates," Appl. Opt. **24**, 1680-1683 (1984).

11. R. Thurn, and W. Kiefer, "Structural resonances observed in the Raman spectra of optically levitated liquid droplets," Appl. Opt. **24**, 1515-1519 (1985).

12. J. D. Eversole, H. B. Lin, and A. J. Campillo, "Cavity-mode identification of fluorescence and lasing in dye-doped microdroplets," Appl. Opt. **31**, 1982-1991 (1992).

13. L. Collot, V. Lefèvre-Seguin, M. Brune, J. M. Raimond, and S. Haroche, "Very high-Q whispering-gallery mode resonances observed on fused silica microspheres," Europhys. Lett. **23**, 327-334 (1993).

14. R. M. Sayer, R. D. B. Gatherer, R. J. J. Gilham, and J. P. Reid, "Determination and validation of water droplet size distributions probed by cavity enhanced Raman scattering," Phys. Chem. Chem. Phys. **5**, 3732-3739 (2003).

15. P. T. Snee, Y. Chan, D. G. Nocera, and M. G. Bawendi, "Whispering-gallery-mode lasing from a semiconductor nanocrystal/microsphere resonator composite," Adv. Mater. **17**, 1131-1136 (2005).

16. A. Chiasera, Y. Dumeige, P. Féron, M. Ferrari, Y. Jestin, G. Nunzi Conti, S. Pelli, S. Soria, and G. C. Righini, "Spherical whispering-gallery-mode microresonators," Laser Photonics Rev. **4**, 457-482 (2010).

17. L. J. Moore, M. D. Summers, and G. A. D. Ritchie, "Optical trapping and spectroscopic characterisation of ionic liquid solutions," Phys. Chem. Chem. Phys. **15**, 13489-13498 (2013).

18. T. C. Preston and J. P. Reid, "Accurate and efficient determination of the radius, refractive index, and dispersion of weakly absorbing spherical particle using whispering gallery modes," J. Opt. Soc. Am. B **30**, 2113-2122 (2013).

19. R. J. Hopkins, L. Mitchem, A. D. Ward, and J. P. Reid, "Control and characterisation of a single aerosol droplet in a single-beam gradient-force optical trap," Phys. Chem. Chem. Phys. **6**, 4924-4927 (2004).

20. R. E. H. Miles, J. S. Walker, D. R. Burnham, and J. P. Reid, "Retrieval of the complex refractive index of aerosol droplets from optical tweezers measurements," Phys. Chem. Chem. Phys. **14**, 3037-3047 (2012).

21. B. J. Dennis-Smither, R. E. H. Miles, and J. P. Reid, "Oxidative aging of mixed oleic acid/sodium chloride aerosol particles," J. Geophys. Res. **117**, D20204 (2012).

22. B. J. Dennis-Smither, F. H. Marshall, R. E. H. Miles, T. C. Preston, and J. P. Reid, "Volatility and oxidative aging of aqueous maleic acid aerosol droplets and the dependence on relative humidity," J. Phys. Chem. A **118**, 5680-5691 (2014).

23. C. Cai, D. J. Stewart, T. C. Preston, J. S. Walker, Y. H. Zhang, and J. P. Reid, "A new approach to determine vapour pressures and hygroscopicities of aqueous aerosols containing semi-volatile organic compounds," Phys. Chem. Chem. Phys. **16**, 3162-3172 (2014).

24. P. R. Conwell, C. K. Rushforth, R. E. Benner, and S. C. Hill, "Efficient automated algorithm for the sizing of dielectric microspheres using the resonance spectrum," J. Opt. Soc. Am. A **1**, 1181-1187 (1984).

25. S. Hill, C. Rushforth, R. Benner, and P. Conwell, "Sizing dielectric spheres and cylinders by aligning measured and computed resonance locations: algorithm for multiple orders," Appl. Opt. **24**, 2380-2390 (1985).

26. F. A. Jenkins and H. E. White, *Fundamentals of Optics*, 4th ed. (McGraw-Hill, New York, 1976), p. 479.

27. N. R. Draper and H. Smith, *Applied Regression Analysis*, 3rd ed. (John Wiley, New York, 1998), p. 23.

28. P. Debye, "Der lichtdruck auf kugeln von beliebigem material," Ann. Phys. **335**, 57-136 (1909).

29. R. Fuchs and K. Kliewer, "Optical modes of vibration in an ionic crystal sphere," J. Opt. Soc. Am. **58**, 319-330 (1968).

30. J. A. Stratton, *Electromagnetic Theory* (McGraw-Hill, New York, 1941), pp. 556-557.

31. C. Bohren and D. R. Huffman, *Absorption and Scattering of Light by Small Particles* (Wiley Science Paperback, New York, 1998), pp. 100-101.

32. S. Pang, R. E. Beckham, and K. E. Meissner, "Quantum dot-embedded microspheres for remote refractive index sensing," App. Phys. Lett. **92**, 221108 (2008).

33. A. Francois and M. Himmelhaus, "Optical sensors based on whispering gallery modes in fluorescent microbeads: size dependence and influence of substrate," Sensors **9**, 6836-6852 (2009).

34. T. Reynolds, M. R. Henderson, A. François, N. Riesen, J. M. M. Hall, S. V. Afshar, S. J. Nicholls, and T. M. Monro, "Optimization of whispering gallery resonator design for biosensing applications," Opt. Express **23**, 17067 (2015).